Validation of NEMO model against observed trend
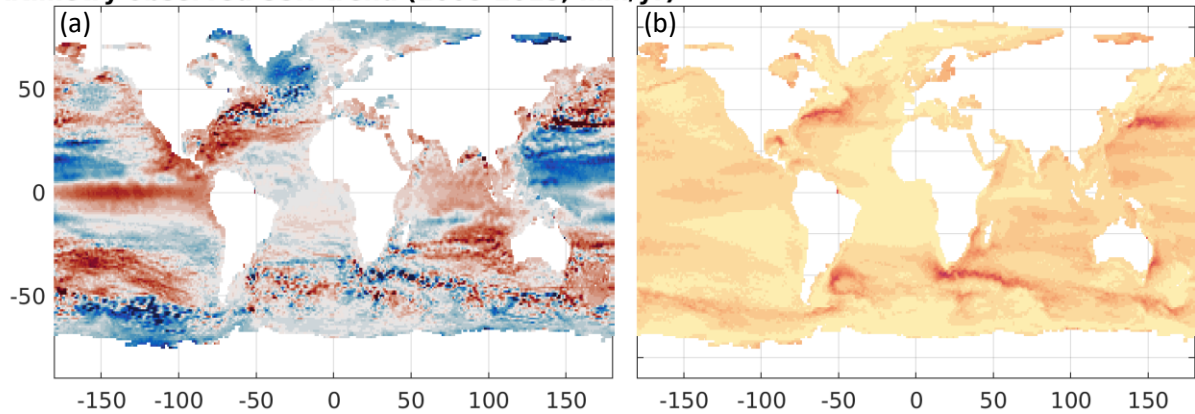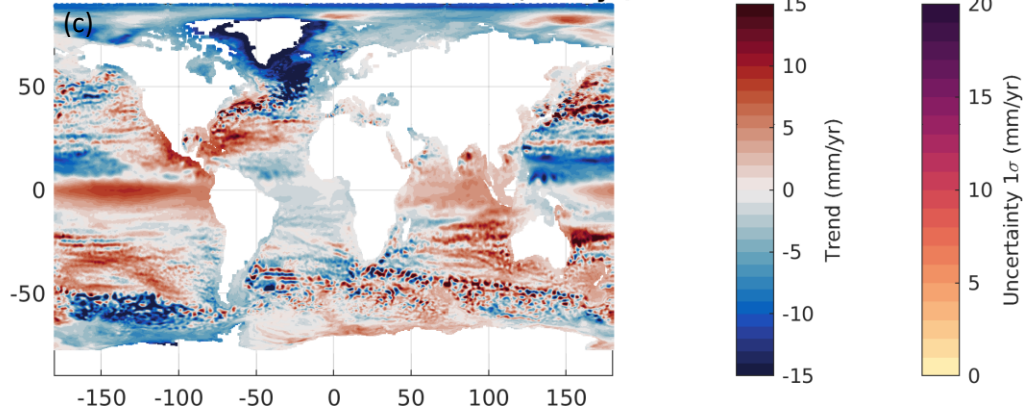
Figure S1. The linear trend from 2005—2015 inclusive for satellite altimetry observations (AVISO, 2020) the decadal trend (a) and its uncertainty assuming an auto-regressive lag-1 noise (b) and the NEMO model plus GRD geoid spatial redistribution (Frederikse et al., 2020) (c).

Supplementary Information to "Attributing decadal-scale climate variability in coastal sea-level trends" by S. Royston, R. J. Bingham and J. L. Bamber

Climate index time series and trends
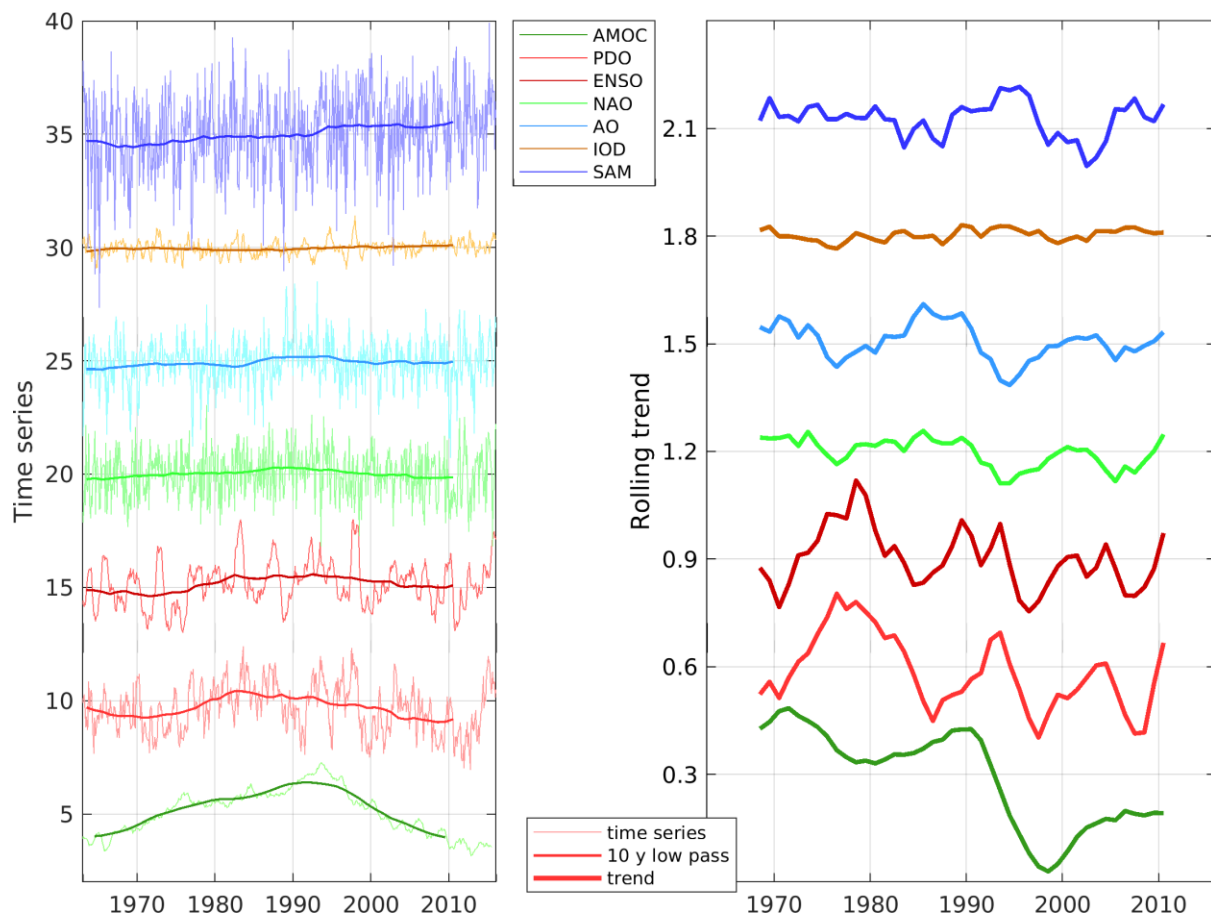
Figure S2. The time series (left) and decadal trends (right) of leading climate indices used in this study (see main text for the data citations).

Primary modes of variability in decadal trends

Taking the global, coastal ocean, the first principal component of SSH, steric sea level and manometric sea level all correlate well (statistically significant to 95 or 99\%) with decadal trends in the PDO (Supplementary Information). Hence globally, the PDO dominates the decadal-scale variability of coastal sea level over other climate processes, which has been shown before (Hamlington etal., 2013; Nerem et al. 2018).

Because the PDO or ENSO decadal variability dominate the power in sea level variability, the EOF bases on a global data set are forced to be orthogonal to that mode. To investigate other drivers, we further mask the data into three oceanic basins, the Atlantic, Pacific and Indian Oceans. By focusing on each oceanic basin in turn, the dominant mode(s) from each region can be identified.

For the total SSH signal which includes GRD, the first principal component and its spatial pattern varies by basin, with the decadal rolling trends in the ENSO index having highest Pearson's correlation coefficient with PC1 in the Pacific and Indian Ocean basins but the Atlantic Ocean coastal sea level having highest correlation with the AO (Figure S3). It is notable that over the decadal timescales investigated here, the correlation of ENSO (and PDO, not shown) is diminished between

Supplementary Information to "Attributing decadal-scale climate variability in coastal sea-level trends" by S. Royston, R. J. Bingham and J. L. Bamber

the Pacific and Indian Ocean, that the time-lag in the El Nino or La Nina type disturbance leading to a sea level disturbance through the Indonesian Throughflow is not apparent but there are peaks and troughs in the PC1 in the Indian Ocean that are not related to ENSO, particularly since 2000. It is notable that the sea-level trend pattern (EOF1) in the Atlantic Ocean is dominated by north-south bipole signals on both the east and west of the basin. An increasing (decreasing) trend in the AO can be associated with a negative (positive) sea level trend in the Baltic Sea and a positive (negative) trend in the far Eastern Mediterranean and Black Seas. An increasing (decreasing) trend in the AO can be associated with a positive (negative) trend on the US and Canadian Atlantic coasts north of Chesapeake Bay and a negative (positive) trend on the oceanward east-facing coast of The Bahamas and Greater Antilles of the Caribbean islands. Large positives on the south-east Greenland and Iceland coasts which are dominated by GRD effects (Figure S3).
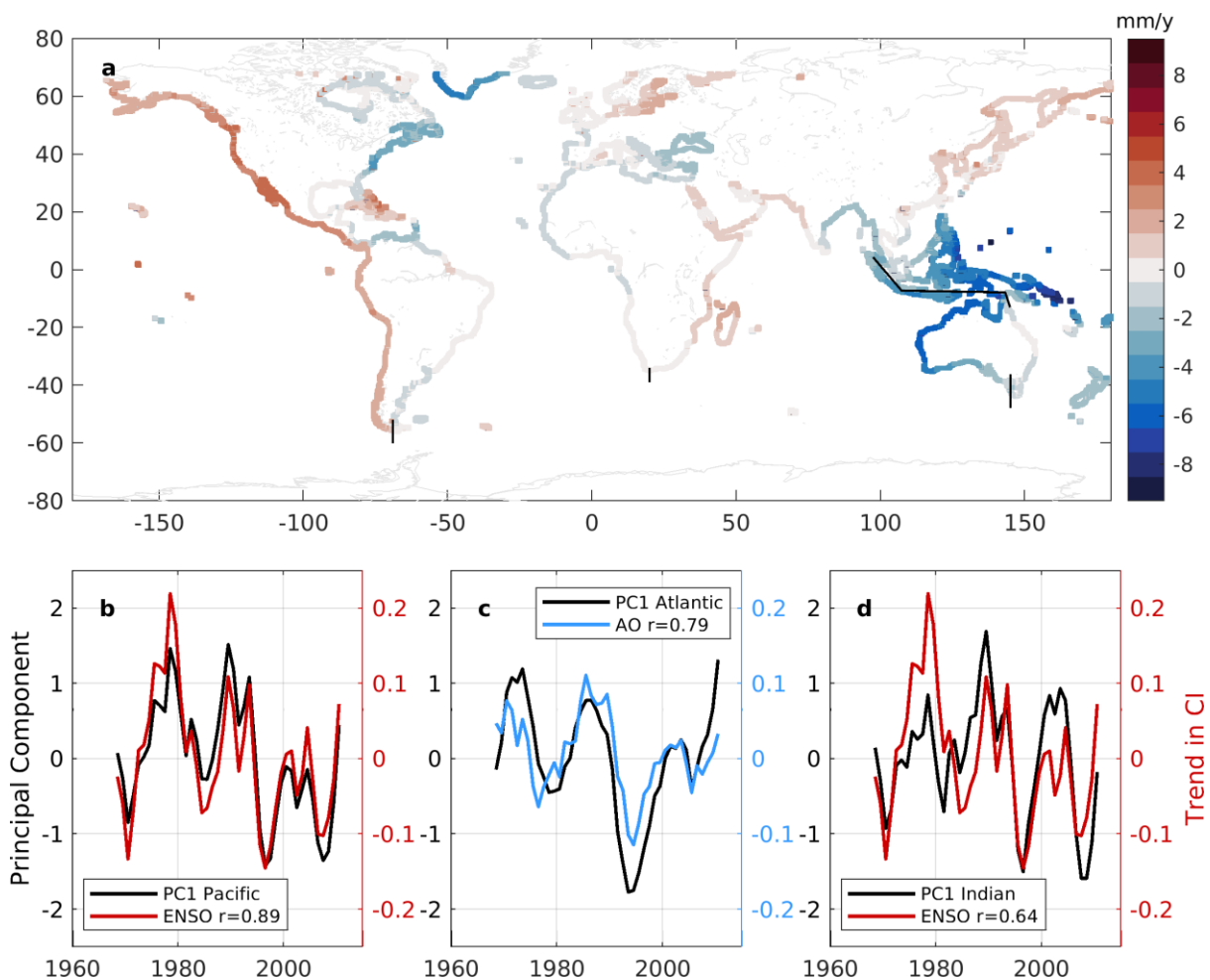
Figure S3. The spatial pattern (a) and rolling decadal trend PC1 for the Pacific (b), Atlantic (c), and Indian (d) Ocean basins shown with the climate index with highest correlation, for SSH.

The sea-level trend reconstruction presented in Figures 3 and 4 uses a linear combination of reconstructed PC modes for each basin and for each steric, manometric and GRD component, with the coefficient of the linear regression given in Table S1 for the Atlantic, Pacific and Indian basins respectively. Following which, the EOF patterns and PC time series are presented where applicable in Figures S4-S17.

Supplementary Information to "Attributing decadal-scale climate variability in coastal sea-level trends" by S. Royston, R. J. Bingham and J. L. Bamber

	Atlantic		Pacific		Indian	
	Index	**Beta**	**Index**	**Beta**	**Index**	**Beta**
Steric						
PC1	AMOC	-0.830	ENSO	1.602	ENSO	-0.948
PC2	-	-	SAM	2.305	AMOC	-0.539
PC3	AO	2.274	AO	-1.161	SAM	-1.700
PC4	ENSO	-0.710	PDO	-0.768	AO	-1.213
PC5	-	-	AMOC	-0.606		
PC6	ENSO	-1.108				
Manometric						
PC1	AMOC	-1.013	ENSO	1.641	ENSO	-1.239
PC2	AO	1.828	AO	-1.955	PDO	-0.677
PC3	PDO	-0.812	-	-	AO	-1.438
PC4	IOD	-3.807	-	-	-	-
PC5			IOD	5.134		
GRD						
PC1	AMOC	-0.666	AMOC	-0.881	AMOC	-0.839
PC2			ENSO	0.839	SAM	1.808
PC3					ENSO	0.730

Table S1. The linear trend coefficient between decadal trend in climate index and PC time series, for PCs contributing up to 95% of variance explained (shading denotes where the PC describes less than 5% variance explained and is omitted) and only included when the relationship is statistically significant against a t-test (hyphen denotes t-test cannot reject the null hypothesis).
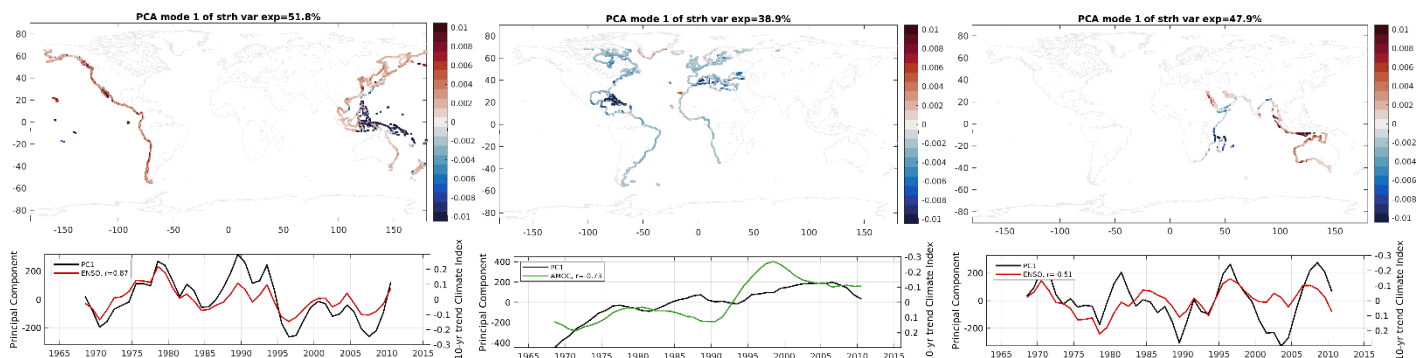
Figure S4. Steric PC1 spatial pattern (a) and rolling decadal trend (b).
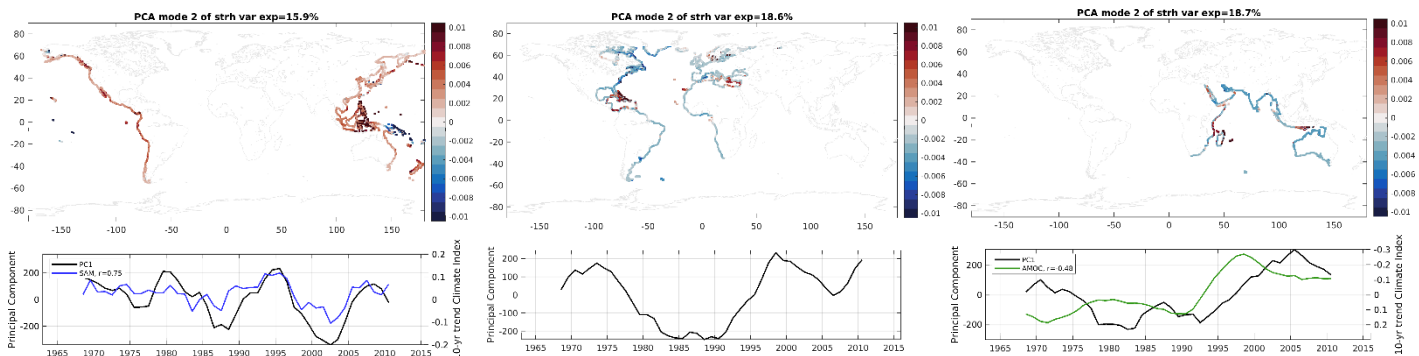
Figure S5. Steric PC2 spatial pattern (a) and rolling decadal trend (b). This pattern is ignored in the Atlantic basin in the reconstruction.

Figure S6. Steric PC3 spatial pattern (a) and rolling decadal trend (b).
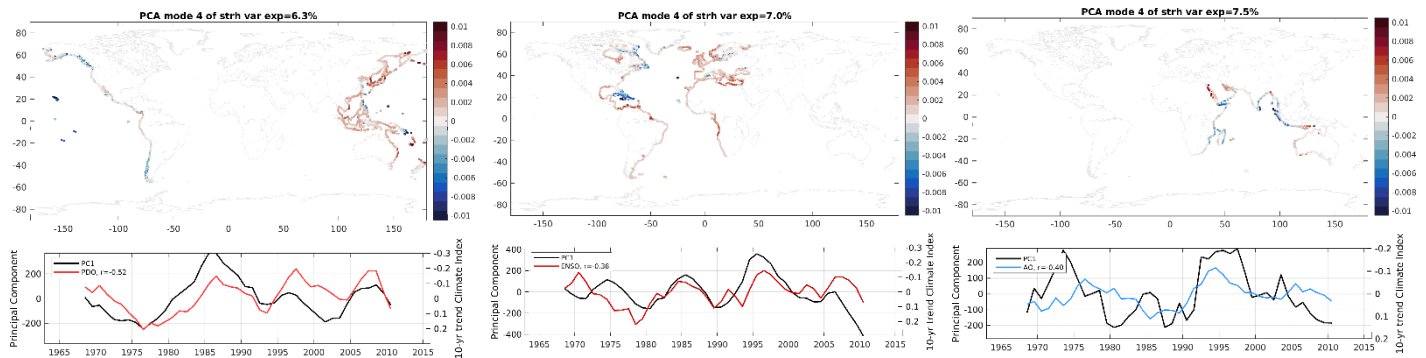
Figure S7. Steric PC4 spatial pattern (a) and rolling decadal trend (b).
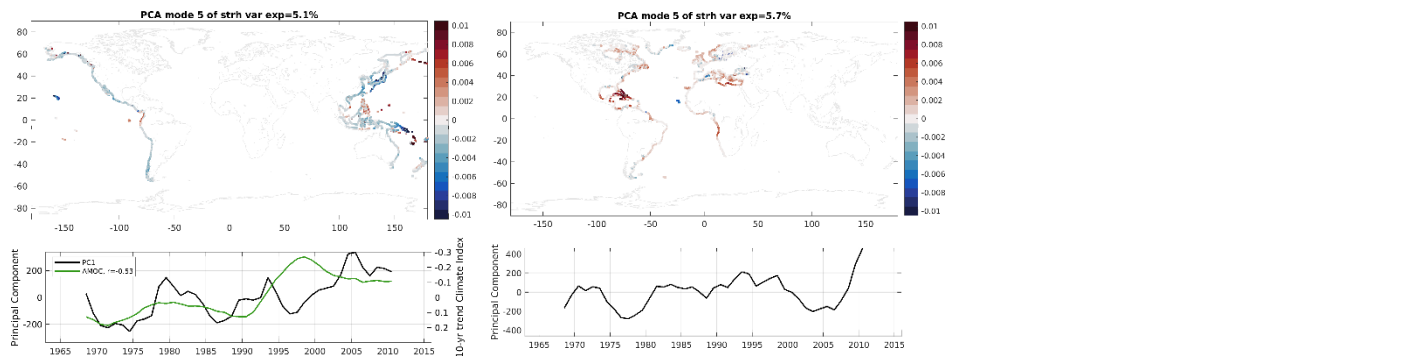
Figure S8. Steric PC5 spatial pattern (a) and rolling decadal trend (b). This pattern is ignored in the Atlantic and Indian basins in the reconstruction.
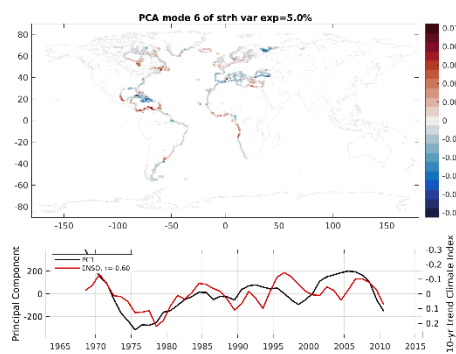
Figure S9. Steric PC6 spatial pattern (a) and rolling decadal trend (b). This pattern is ignored in the Pacific and Indian basins in the reconstruction.

Supplementary Information to "Attributing decadal-scale climate variability in coastal sea-level trends" by S. Royston, R. J. Bingham and J. L. Bamber
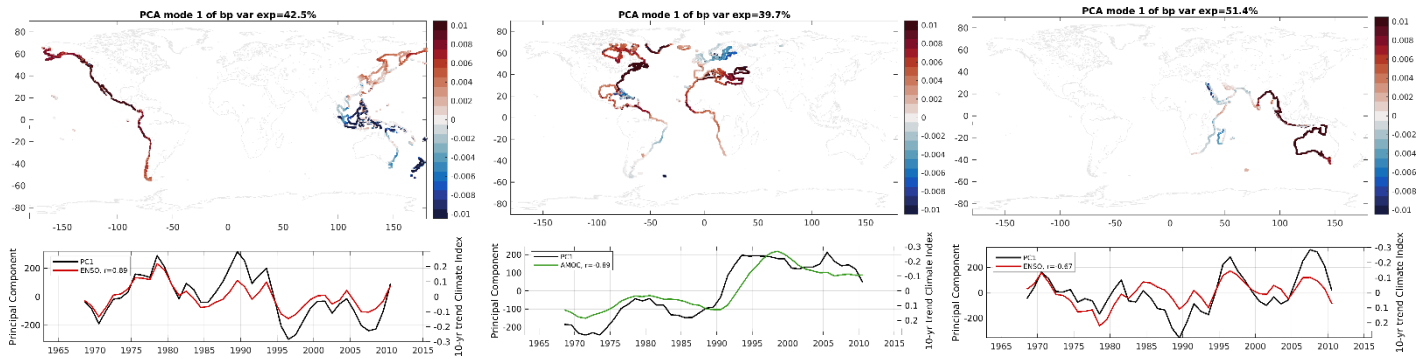
Figure S10. Manometric PC1 spatial pattern (a) and rolling decadal trend (b).
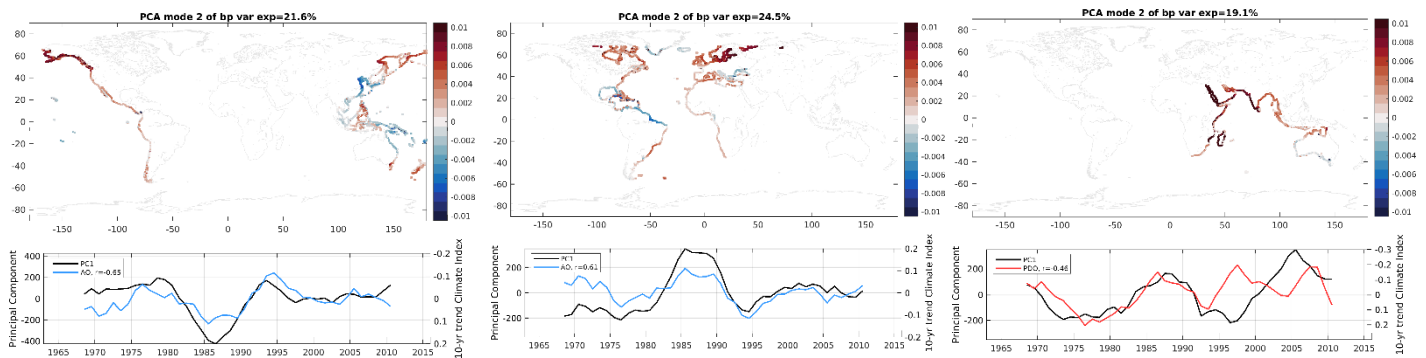
Figure S11. Manometric PC2 spatial pattern (a) and rolling decadal trend (b).
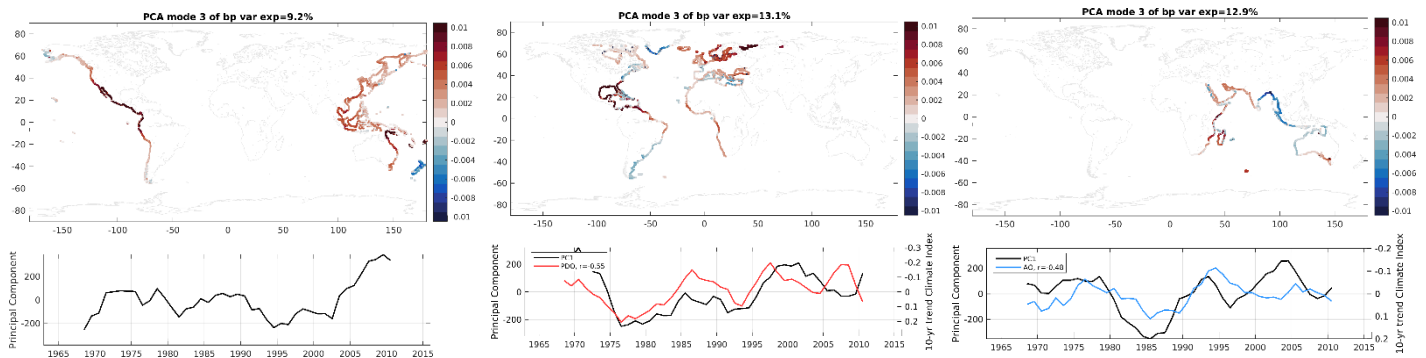
Figure S12. Manometric PC3 spatial pattern (a) and rolling decadal trend (b). This pattern is ignored in the Pacific basin in the reconstruction.
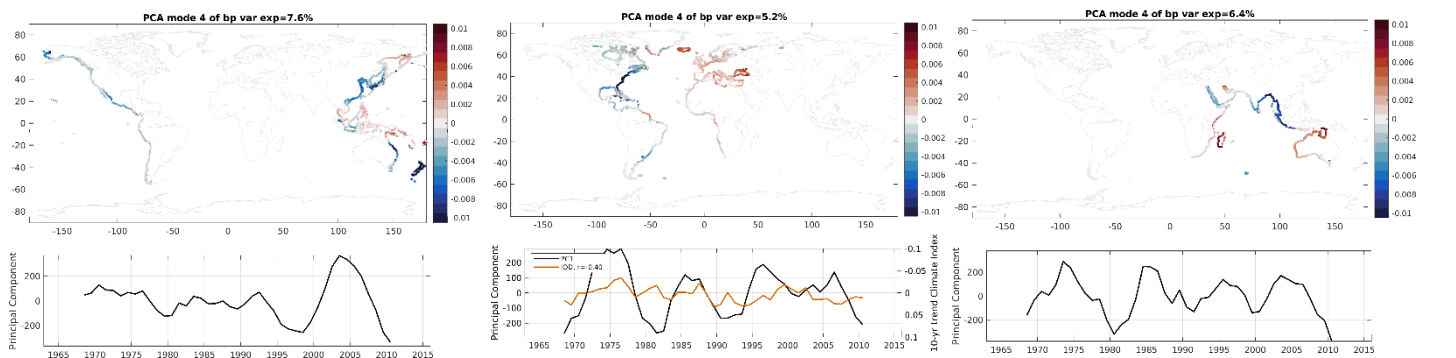
Figure S13. Manometric PC4 spatial pattern (a) and rolling decadal trend (b). This pattern is ignored in the Pacific and Indian basins in the reconstruction.
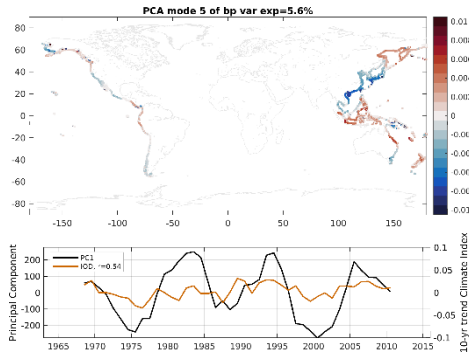
Figure S14. Manometric PC5 spatial pattern (a) and rolling decadal trend (b). This pattern is ignored in the Atlantic and Indian basins in the reconstruction.
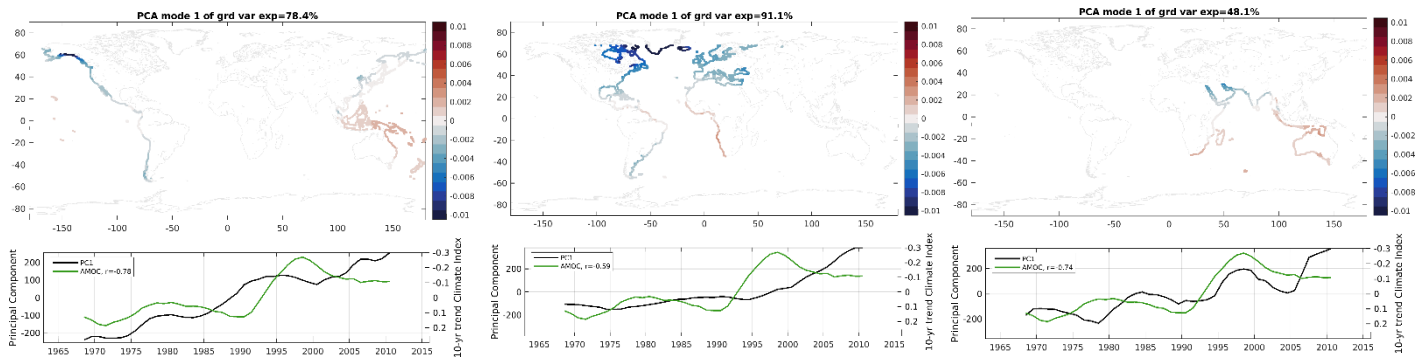
Figure S15. GRD PC1 spatial pattern (a) and rolling decadal trend (b).

Figure S16. GRD PC2 spatial pattern (a) and rolling decadal trend (b). This pattern is ignored in the Atlantic basin in the reconstruction.
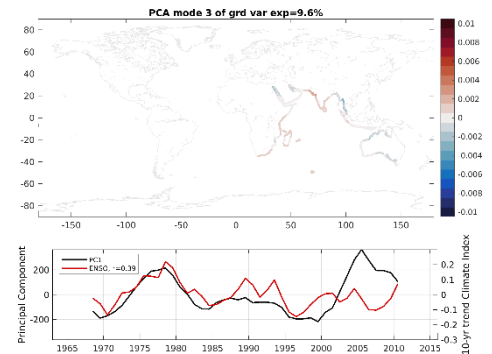
Figure S17. GRD PC3 spatial pattern (a) and rolling decadal trend (b). This pattern is ignored in the Atlantic and Pacific basins in the reconstruction.